Article

Applications of Terrestrial Laser Scanner in Detecting Pavement Surface Defects

Abdelhalim Azam [1,*], Abdulaziz H. Alshehri [2,*], Mohammad Alharthai [2], Mona M. El-Banna [3], Ahmed M. Yosri [1] and Ashraf A. A. Beshr [4,5]

1   Department of Civil Engineering, College of Engineering, Jouf University, Sakaka 72388, Saudi Arabia; amyosri@ju.edu.sa
2   Department of Civil Engineering, College of Engineering, Najran University, Najran 66446, Saudi Arabia; maalharthai@nu.edu.sa
3   Civil Engineering Department, Kafrelshikh University, Kafrelshikh 33516, Egypt
4   Public Works Department, Faculty of Engineering, Mansoura University, Mansoura 35511, Egypt; aaabeshr@mans.edu.eg
5   Civil Engineering Department, Delta Higher Institute for Engineering and Technology, Mansoura 35681, Egypt
*   Correspondence: amazam@ju.edu.sa (A.A.); ahalshehry@nu.edu.sa (A.H.A.)

Abstract: An entire roadway system represents a crucial element in the sustainable urban transportation planning process. Pavement surfaces are at continual risk of accumulating serious deteriorations and defects throughout their service life due to traffic loading and environmental impact. Since roadway networks are growing rapidly, relying on visual pavement inspection is not always feasible. Therefore, this paper proposes an effective assessment method for evaluating flexible pavement surface distresses using a terrestrial laser scanner (TLS) and calculating the pavement condition index (PCI). The proposed terrestrial laser scanner method results in road condition assessments becoming faster, safer, and more systematic. It also aims to determine the geometric characteristics of the investigated roads. A major road in Egypt was selected to test the proposed technique and compare it with the traditional visual inspection method. The evaluation was carried out to assess different types of pavement distress, such as cracking, rutting, potholes, and raveling distresses. Every pavement distress was defined in terms of surface area, the width of the crack, and intensity, and the data from TLS were then processed by MAGNET COLLAGE software. A MATLAB program was developed to match the TLS observational data to plane equations. PAVER software was also used to determine the PCI values for each TLS position. The revealed distresses for the investigated road using TLS observations reveal a significant improvement in determining flexible pavement distresses and geometric characteristics.

Keywords: laser scanner; flexible pavement; plane equation; pavement distress; PCI

1. Introduction

The structural design of flexible pavement is a function of traffic loads, climate conditions, the construction materials' mechanical properties, and the soil subgrade's stiffness [1–3]. The flexible pavement sections are constructed from bituminous surface materials and unbound granular materials. The loading stresses transfer to the subgrade soil through the different pavement layers. The wearing surface layer is often bituminous material. Due to the viscous nature of asphalt, significant plastic deformation results from traffic movement and climatic factors, which has an impact on pavement life.

Pavement distress is usually caused due to improper maintenance, unsuitable construction material, excess traffic loads, poor surface drainage, and climate conditions such as frost [4]. Consequently, the traffic speed and safety decrease, resulting in more fuel consumption and increased trip times. In addition, any defect in the pavement surface makes

the road unsafe and inconveniences users [5]. Consequently, regular inspections should be conducted by the responsible agencies to assess pavement conditions and determine a reasonable maintenance program. It is important to identify road distress early in order to conduct road maintenance before the distress worsens or the pavement surface becomes completely unsuitable for use. Regular road maintenance results in extending pavement service life and decreased maintenance costs [6]. When using manual inspection for determining road conditions, the inspector must move along the road to discover the possible distress, a process that is considered costly and represents a traffic hazard. Therefore, there is a need for automated distress detection systems for assessing the quality of road surfaces.

Several methods can be applied to evaluate the pavement conditions, such as the pavement condition rating (PCR), pavement condition index (PCI), and international roughness index (IRI) [7,8]. The PCI method is a numerical evaluation of pavement quality based on the degree of severity and density of the surface distresses. It is well known that determining the exact causes of certain distresses can be difficult but these can be recognized by a correct understanding of the interactions between the flexible pavement, environmental conditions and traffic levels [9]. In addition, several studies have predicted pavement performance using the available software such as AASHTOWare pavement ME design software and quality-related specification software (QRSS) [1,2,10–14]. Asphalt concrete (AC) rutting and bottom-up fatigue cracking are the predicted problems. Performing field surveys is essential for the calibration of these prediction techniques.

Because of digitization trends, significant advancements in geodesy and image-processing technologies have occurred. The various tools for digital image processing, such as terrestrial laser scanners (TLS), photogrammetry, and automatic and robotic geodetic equipment, have been applied in many disciplines of civil engineering [15,16]. In recent years, the laser scanning technique has been applied with digital photogrammetry for 2D and 3D modeling instead of conventional modeling techniques. Laser scanners have the advantage that they can develop a cloud network through three steps in a three-dimensional imaging process and then combine these using a program. Furthermore, the details of the objects (internal and external) can be measured by imaging them as point sequences in the vertical and horizontal directions at a specific angle, which is the most widely used technique in image measurement and involves sequential images and the measurement of a three-dimensional model [17]. Laser scanning technology became widely used in response to safety issues, aiming for risk reduction regarding climbing and burns from chemical exposure, as well as a reduction in the time required for data collecting. It can drastically reduce the amount of time needed for field measurements as well as the inaccuracies associated with conventional field measurements [18].

3D laser scanning technology is a new and advanced monitoring technology used in civil engineering applications, which has the capability to produce a cloud of three-dimensional points that can be utilized in measuring road defects. Two categories of 3D laser scanners exist: time-of-flight laser scanners and phase-shift laser scanners. Time-of-flight laser scanners produce a laser light pulse that is inverted on the target object. The sensor inside the device calculates the optical pulse's time of flight after being reflected on the surface. This type of device can repeatedly determine when an emitting pulse's signal arrives. In phase-shift scanners, a laser beam with sinusoidally modulated optical power is discharged and mirrored on the target object. The phase shift is then determined by measuring the reflected light and contrasting it with the emitted light [16]. By monitoring the phase difference between the emitted and reflected signals and the phase shift, 3D scanners can calculate the distance to an item. Phase-shift scanners operate at lower ranges than time-of-flight scanners, typically between 1 and 50 m and up to a maximum of 80 to 120 m [16].

Several studies have employed the TLS technique in determining pavement surface distress [19–23]. Feng et al. [19] used TLS point clouds to determine five pavement distresses. In similar studies, El Issaoui et al. [20] and De Blasiis et al. [24], and Lueangvilai [25] investigated the feasibility of using mobile laser scanning (MLS) system for measuring rut-

ting depth and road slope for pavements system. The authors used the TLS measurements as a reference for MLS. The findings reported that using MLS is precise and functional for applications. Yi and Ahmad [26] evaluated using TLS and unscrewed aerial vehicles to determine road crack mapping. Based on the results, it was found that TLS is more accurate and reliable. Bitelli et al. [21] evaluated the application of laser scanner techniques for determining the texture characteristics of different types of asphalt mixtures. The authors concluded that the Laser scanners could be applied on a real surface layer through a single measurement.

Different factors can result in flexible pavement deterioration and should be considered in the design of road systems, such as the failure of subgrade, subbase, or base and wearing course [27]. Road deterioration results from bad construction or design, natural wear and tear during the pavement life, changes in climate conditions, and excessive traffic loads. Pavement design is a two-step process that determines the most cost-effective combination of pavement materials, material mixture design for each pavement layer, and pavement structural design (ii) (thickness design and type of different component layers). Climate conditions, road geometry, traffic loads, location, and subgrade soil and drainage are all important aspects to consider during pavement design. Tarawneh and Sarireh [28] confirmed that damage to flexible pavements is due to traffic loads and climatic influences. This effect is influenced by the properties of construction materials and construction technology during road construction, but traffic loads and volumes influence the most significant impacts. The strength of the pavement is also reduced when the moisture content rises, and poor drainage contributes to pavement collapse. In a new experimental mechanical design approach, the evaluation of error prediction and crack reliability was looked into. The manual looked at design parameters for traffic levels, substrate, environment, and reliability for different pavements [29–31]. McGhee [32] created a new method for quickly gathering data utilizing 3D laser technology, and field testing was used to determine the method's viability. Many studies were conducted to investigate this topic. Jung and Zollinger [33] built a model for experimental mechanical error that was calibrated using the results of a new wear test and long-term pavement performance data. On the other hand, Mraz et al. [34] proposed the automated error technique.

In Egypt, this technique is almost new. This study tries to apply it to determine the pavement defects and geometric characteristics instead of the traditional methods, which are considered costly and require a long time. Also, there is still a need for an optimal method to accurately identify road defects to determine the optimum method for pavement maintenance programs.

This research is a trial of applying the TLS as a new and accurate geodetic technique in detecting flexible pavement surface defects for a major road in Egypt. Three-dimensional TLS was applied for scanning Kafr El-Sheikh-Tanta road and developing a 3D model for flexible pavements road through eight positions scans. Thus, the specific objectives are to:

(a) Detect and estimate the flexible pavement surface defects and the geometric characteristics of the investigated road based on the TLS observations.
(b) Compare the measurement of pavement distresses by traditional techniques (visual inspection) with the prediction of defects by TLS.
(c) Finally, determine the pavement condition index (PCI) for the investigated road using the TLS technique.

2. Research Methodology

The main benefit of using a TLS system is that it improves the measuring range and balance to achieve high accuracy and efficiency-enhanced speed by measuring process time of flight with better speed, accurate scan technology, and implementing high-speed imaging in all fieldwork processes and data collection. Five different measurement modes are available, three of which can be used for different applications. Special features in laser scanning applications aid ease of use, security, and safety. Topcon GLS-2000 3D TLS was employed for data collection and site work.

The TLS is being used as a horizontal measurements can angle of 360° and 270°, and it can capture point clouds for real objects that are challenging to measure, such as historical buildings, bridges, high-rise buildings, roads, etc. It also has a dual camera, a 170° wide-angle camera (5 megapixels), and an 8.9° narrow-angle camera (5 megapixels) positioned in coaxial alignment with the measuring axis. With a distance precision of 2 mm, the scanning range reaches up to 350 m. The compensation range is ±6 min, and the target detection accuracy reaches 3 s at 50 m. It takes at most 18 min to obtain a 5 million scanned points cloud with a 6-s angular resolution. The accuracy of the Topcon GLS-2000 instrument was verified by conducting some laboratory tests before recording the fieldwork and data collection.

Before utilizing the specified TLS, several setting modifications were made. To conduct data post-processing, the target object was first aligned with the spot information of numerous 3D imaging data. Then, the target was positioned in a place that allowed the detection of all defects in this position and placed close to the scanning target for measuring the object. The target was placed in several positions to align the positional information with the data, as shown in Figure 1. Three separate road system scans were performed depending on the various instrument placements; each scan has a different scan mode, scan resolution, time of the scan, and, consequently, the number of observed points than the other scans, as presented in Table 1.
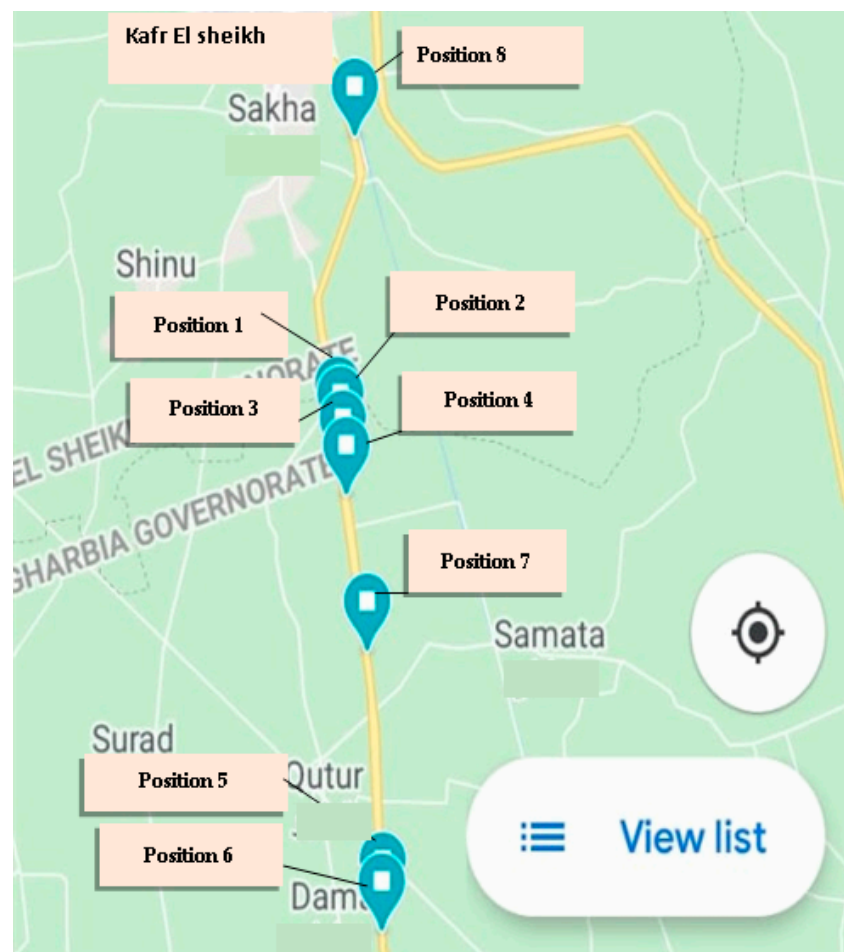

Figure 1. Different positions of Topcon GLS-2000Laser Scanner.

Table 1. Properties of all TLS scans using Topcon GLS-2000 instrument (Eight instrument positions and 10 scans).

Laser Scanner Positions	TLS Mode of Scan	Scan Resolution/Distance	Scan Time (min)	Distance (From the Beginning of Road), km
First	Road mode	3.1 mm/40 m	1.53	0.00 (From Kafr El-Sheikh city)
Second (1)		1.6 mm/25 m	3.43	5.89
Second (2)	Standard mode	1.2 mm/10 m	3.24	5.89
Second (3)	Standard mode		9.50	5.89
Third		1.6 mm/25 m	6.34	6.574
Fourth		3.1 mm/40 m	2.50	7.117
Fifth	Road mode		7.00	10.277
Sixth			5.59	15.476
Seventh		1.6 mm/25 m	6.46	15.888
Eighth			6.45	20.125

Table 1 shows the type, the number of scanning positions, the distance of each position scan, and the scan resolution for each TLS location. The scan resolution is measured in millimeters for each distance and depends on the scan time. Additionally, the resolution of the scanner influences this number, with higher resolutions requiring longer scan times (eight instrument positions and 10 scans). The point clouds of each TLS position have been processed using the software programming Magnet, thus obtaining 10 sub-clouds that describe the distresses on the surface of the studied road.

The MAGNET Collage program can handle laser scanners, portable scanners, mapping road resurfacing scanners, and picture point retractions. Further streamlining data collection is the fast matching of point clouds from sweep control and ground control using geographic coordination points. With precise measuring and annotation capabilities such as split screen, filtered views, and linear spacing, it also offers a fantastic browsing experience [35,36]. The collected data resulting from TLS observations were processed using the MAGNET COLLAGE program to measure the surface defects with high accuracy, as demonstrated in Figure 2. It should be noted that the images in Figure 2 were generated by MAGNET program based on TLS observations, and the images are 3D point cloud. The difference in colors in these images represents a change in the levels of these points, which facilitates the measurement process from each image.

The terrestrial laser scanner technique is available in several construction companies and educational institutes in Egypt. The applied software for TLS data processing is provided with the instrument, and several well-trained technicians can use this technique well. The use of the laser scanner in determining pavement distress can be finished in a few hours. The technician's salary is almost the same compared to the other traditional methods. On the other hand, using the traditional method for determining pavement defects requires time and effort. It may be unsafe during the inspection due to the movement of traffic volumes.

2.1. Analysis of Terrestrial Laser Scanner Observations

The Cartesian coordinates (X, Y, Z) for any observed point (i) from basic measurements of laser scanner observations and their accuracy should be calculated as follows [12]:

$$\left. \begin{array}{l} X_i = S\cos\gamma\sin\alpha; \\ Y_i = S\cos\gamma\cos\alpha; \\ Z_i = S\sin\gamma \end{array} \right\} \tag{1}$$

where:

S, α, γ—the measured distance, horizontal and vertical angles (in degree), respectively.
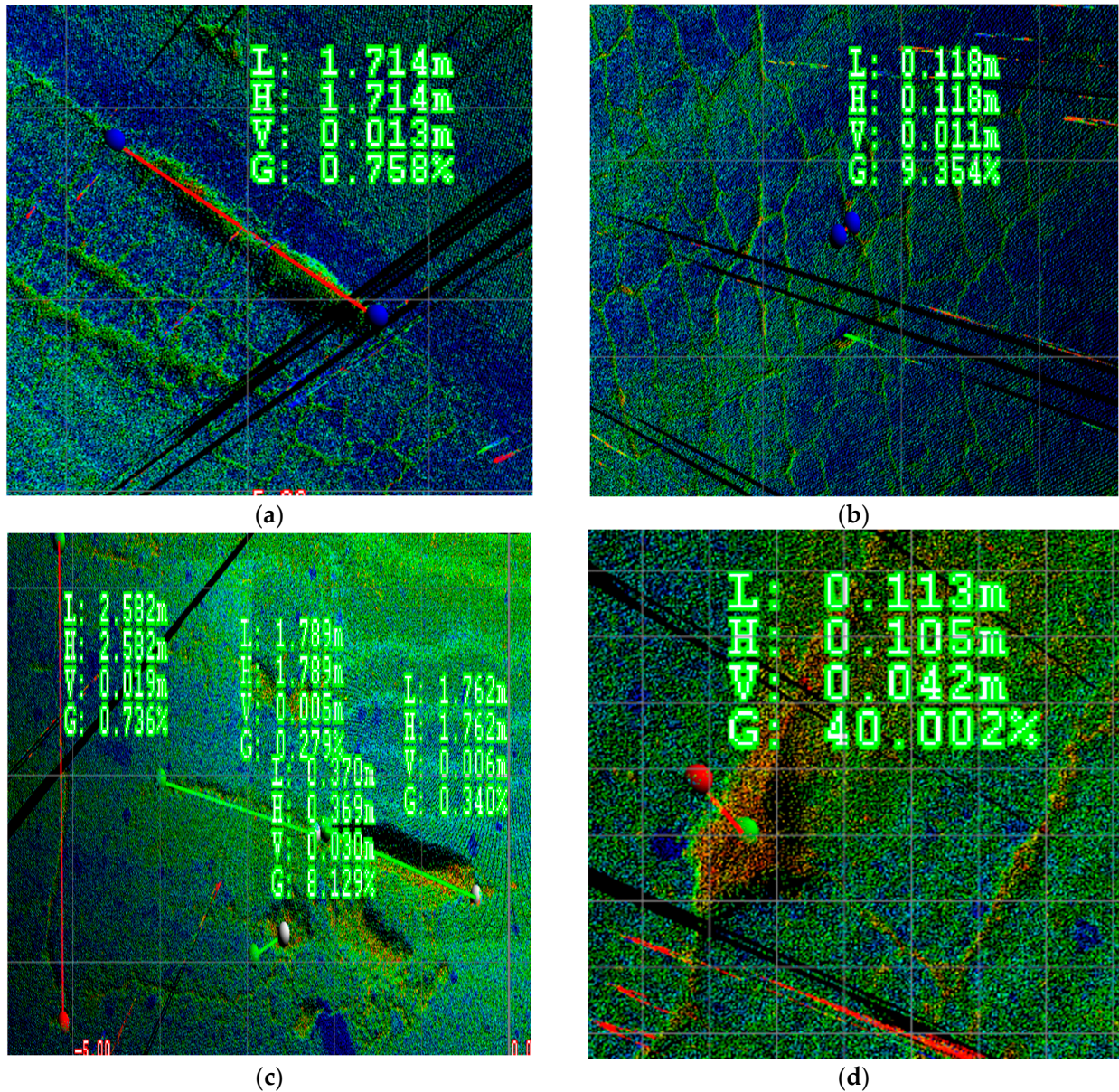
Figure 2. Examples of TLS-generated points clouds after data processing. (**a**) Longitudinal cracking in pos. 5, (**b**) Alligator cracking in pos. 6, (**c**) Longitudinal cracking and potholes, (**d**) Depth of pothole in pos.3.

Because there are no observations of redundancy in Equation (1), there is only one solution, and thus the multivariate error propagation technique can be applied to calculate the point coordinates accurately.

$$
\left.
\begin{aligned}
m_X^2 &= \left(\frac{X}{\sqrt{X^2+Y^2+Z^2}}\right)^2 m_S^2 + (Y)^2 m_\alpha^2 + \left(\frac{ZX}{\sqrt{X^2+Y^2}}\right)^2 m_\gamma^2; \\
m_Y^2 &= \left(\frac{Y}{\sqrt{X^2+Y^2+Z^2}}\right)^2 m_S^2 + (X)^2 m_\alpha^2 + \left(\frac{ZY}{\sqrt{X^2+Y^2}}\right)^2 m_\gamma^2; \\
m_Z^2 &= \left(\frac{Z}{\sqrt{X^2+Y^2+Z^2}}\right)^2 m_S^2 + \left(\sqrt{X^2+Y^2}\right)^2 m_\gamma^2.
\end{aligned}
\right\}
\tag{2}
$$

where:

m_S, m_α, m_γ—standard deviation of the measured distance, the standard deviation of vertical and horizontal angles of the used laser scanner.

The values m_S, m_α, m_γ should be calculated experimentally or can be taken from the instrument specifications.

Because of laser scanner observations, the following road elements can be identified based on the adjusted coordinates and their accuracy.

The direct distance between any two observed points (i, j) resulting from TLS observations can be calculated using the following formula [16]:

$$D = \sqrt{\left(x_j - x_i\right)^2 + \left(y_j - y_i\right)^2 + \left(z_j - z_i\right)^2} \tag{3}$$

The accuracy of the measured distance (m_D) can be determined using the Jacobian method by differentiating Equation (3) as follows:

$$\left. \begin{aligned} m^2{}_D &= (\tfrac{x_j - x_i}{D})^2 m^2_{X_j} + (\tfrac{x_i - x_j}{D})^2 m^2_{X_i} + (\tfrac{y_j - y_i}{D})^2 m^2_{y_j} + (\tfrac{y_i - y_j}{D})^2 m^2_{y_i} + \\ &\quad (\tfrac{z_j - z_i}{D})^2 m^2_{Z_j} + (\tfrac{z_i - z_j}{D})^2 m^2_{Z_i} \end{aligned} \right\} \tag{4}$$

2.2. Calculating Flexible Pavement Deformation Using Equation of Plane

In this paper, the technique used in determining flexible pavement deformation of the studied road depends on dividing the total point cloud resulting from laser scanner observations into sub-clouds for each instrument position. The roadway surface can be represented for each instrument position by a plane that interpolates the clouds both for the apron (general plane) and for each instrument position (local plane). As a result, any distortion in the resulting plane should be considered road deformation. The following is the plane equation derived from TLS scanner observations:

The plane equation can be calculated using the coordinates of three points lying on this plane, which has (X_1, Y_1, Z_1), (X_2, Y_2, Z_2), (X_3, Y_3, Z_3) as follows [16]:

$$A.X + B.Y + C.Z + D = 0 \tag{5}$$

The coefficients (A, B, C and D) of Equation (5) should be calculated by the following equations [12]:

$$\left. \begin{aligned} A &= Y_1(Z_2 - Z_3) + Y_2(Z_3 - Z_1) + Y_3(Z_1 - Z_2); \\ B &= Z_1(X_2 - X_3) + Z_2(X_3 - X_1) + Z_3(X_1 - X_2); \\ C &= X_1(Y_2 - Y_3) + X_2(Y_3 - Y_1) + X_3(Y_1 - Y_2); \\ D &= -X_1(Y_2Z_3 - Y_3Z_2) - X_2(Y_3Z_1 - Y_1Z_3) - X_3(Y_1Z_2 - Y_2Z_1). \end{aligned} \right\} \tag{6}$$

The accuracy of coefficients (A, B, C, and D) should be calculated using error propagation through differentiation of Equation (6) based on the accuracy of the coordinates as shown below:

$$\left. \begin{aligned} m^2{}_A &= (Z_2 - Z_3)^2 m_{Y_1}{}^2 + (Z_3 - Z_1)^2 m_{Y_2}{}^2 + (Z_1 - Z_2)^2 m_{Y_3}{}^2 + (Y_3 - Y_2)^2 m_{Z_1}{}^2 + (Y_1 - Y_3)^2 m_{Z_2}{}^2 + (Y_2 - Y_1)^2 m_{Z_3}{}^2; \\ m^2{}_B &= (Z_3 - Z_2)^2 m_{X_1}{}^2 + (Z_1 - Z_3)^2 m_{X_2}{}^2 + (Z_2 - Z_1)^2 m_Y{}^2 + (X_2 - X_3)^2 m_{Z_1}{}^2 + (X_3 - X_1)^2 m_{Z_2}{}^2 + (X_1 - X_2)^2 m_{Z_3}{}^2; \\ m^2{}_C &= (Y_2 - Y_3)^2 m_{X_1}{}^2 + (Y_3 - Y_1)^2 m_{X_2}{}^2 + (Y_1 - Y_2)^2 m_{X_3}{}^2 + (X_3 - X_2)^2 m_{Y_1}{}^2 + (X_1 - X_3)^2 m_{Y_2}{}^2 + (X_2 - X_1)^2 m_{Y3}{}^2; \\ m^2{}_D &= (Y_3Z_2 - Y_2Z_3)^2 m_{X_1}{}^2 + (Y_1Z_3 - Z_1Y_3)^2 m_{X_2}{}^2 + (Y_2Z_1 - Y_1Z_2)^2 m_{X_3}{}^2 + (X_2Z_3 - X_3Z_2)^2 m_{Y_1}{}^2 + \\ &\quad (X_3Z_1 - X_1Z_3)^2 m_{Y_2}{}^2 + (X_1Z_2 - X_2Z_1)^2 m_{Y_3}{}^2 + (X_3Y_2 - X_2Y_3)^2 m_{Z_1}{}^2 + (X_1Y_3 - X_3Y_1)^2 m_{Z_2}{}^2 + \\ &\quad (X_2Y_1 - Y_2X_1)^2 m_{Z_3}{}^2. \end{aligned} \right\} \tag{7}$$

Each instrument position has thousands of point coordinates based on TLS observations. The least-square adjustment technique can be used to determine the plane equation for laser scanner observations (more than three points) as follows:

Equation (5) can be rearranged and written as follows for more than three points lying on the plane [16]:

$$A_1 X_i + B_1 Y_i + C_1 Z_i + D_1 = 0 \tag{8}$$

By dividing the parameters in Equation (8) by C_1, then

$$\frac{A_1}{C_1} X_i + \frac{B_1}{C_1} Y_i + Z_i + \frac{D_1}{C_1} = 0, \tag{9}$$

According to the first principle of least squares, the values of a system of unknown quantities for which observations have been made can be determined with the greatest degree of certainty by reducing the sum of the squares of the errors [16]. Therefore,

$$\left. \begin{aligned} &\sum_{i=1}^{n} V_i^2 = \min; \\ &\sum_{i=1}^{n} \left(Z_i - AX_i - BY_i - C \right)^2 = \min. \end{aligned} \right\} \tag{10}$$

where is the residuals in observations

As a result, to obtain the values of parameters (A, B, C), we have:

$$\left. \begin{aligned} &\frac{\partial}{\partial A} \sum_{i=1}^{n} \left(Z_i - AX_i - BY_i - C \right)^2 = 0.0; \\ &\frac{\partial}{\partial B} \sum_{i=1}^{n} \left(Z_i - AX_i - BY_i - C \right)^2 = 0.0; \\ &\frac{\partial}{\partial C} \sum_{i=1}^{n} \left(Z_i - AX_i - BY_i - C \right)^2 = 0.0 \end{aligned} \right\} \tag{11}$$

At first, the term $\sum_{i=1}^{n} \left(Z_i - AX_i - BY_i - C \right)^2$ can be simplified as follows:

$$\left. \begin{aligned} &\sum_{i=1}^{n} \left(Z_i - AX_i - BY_i - C \right)^2 = \sum_{i=1}^{n} Z_i^2 - 2A \sum_{i=1}^{n} X_i Z_i - 2B \sum_{i=1}^{n} Y_i Z_i - 2C \sum_{i=1}^{n} Z_i + A^2 \sum_{i=1}^{n} X^2 + 2AB \sum_{i=1}^{n} X_i Y_i \\ &+ 2AC \sum_{i=1}^{n} X_i + B^2 \sum_{i=1}^{n} Y_i^2 + 2BC \sum_{i=1}^{n} Y_i + n.C^2 \end{aligned} \right\} \tag{12}$$

So, the following equations can be deduced by differentiating Equation (12) related to the coefficients A, B, and C and then equal to zero [16]:

$$\left. \begin{aligned} &A \sum_{i=1}^{n} X_i^2 + B \sum_{i=1}^{n} X_i Y_i + C \sum_{i=1}^{n} X_i = \sum_{i=1}^{n} X_i Z_i; \\ &A \sum_{i=1}^{n} X_i Y_i + B \sum_{i=1}^{n} Y_i^2 + C \sum_{i=1}^{n} Y_i = \sum_{i=1}^{n} Y_i Z_i; \\ &A \sum_{i=1}^{n} X_i + B \sum_{i=1}^{n} Y_i + n.C = \sum_{i=1}^{n} Z_i \end{aligned} \right\} \tag{13}$$

Equation (13) should be arranged as follows:

$$\begin{bmatrix} A \\ B \\ C \end{bmatrix} = \begin{bmatrix} \sum_{i=1}^{n} X_i^2 & \sum_{i=1}^{n} X_i Y_i & \sum_{i=1}^{n} X_i \\ \sum_{i=1}^{n} X_i Y_i & \sum_{i=1}^{n} Y_i^2 & \sum_{i=1}^{n} Y_i \\ \sum_{i=1}^{n} X_i & \sum_{i=1}^{n} Y_i & n \end{bmatrix}^{-1} \cdot \begin{bmatrix} \sum_{i=1}^{n} X_i Z_i \\ \sum_{i=1}^{n} Y_i Z_i \\ \sum_{i=1}^{n} Z_i \end{bmatrix} \tag{14}$$

When the plane equation from TLS observations for any instrument position is determined by applying the equation mentioned above, the orthogonal distance Δi (distortion in

roadway surface) from any point (i) point to a fitted result from the plane of any instrument position can be calculated [16]:

$$\Delta_i = \frac{AX_i + BY_i + CZ_i - D}{\sqrt{A^2 + B^2 + C^2}}.$$

(15)

3. Field Data Collection

A major road connecting Tanta city and Kafr El-Sheikh city, Egypt, was selected to assess the feasibility of applying TLS in pavement surface distresses. Then a reasonable maintenance program was proposed. The road was reconstructed in two stages and opened for traffic in 2016. The pavement section consists of AC 10 cm and 30 cm base material. The road has three lanes in each direction and a length of approximately 20 km, as shown in Figure 3.
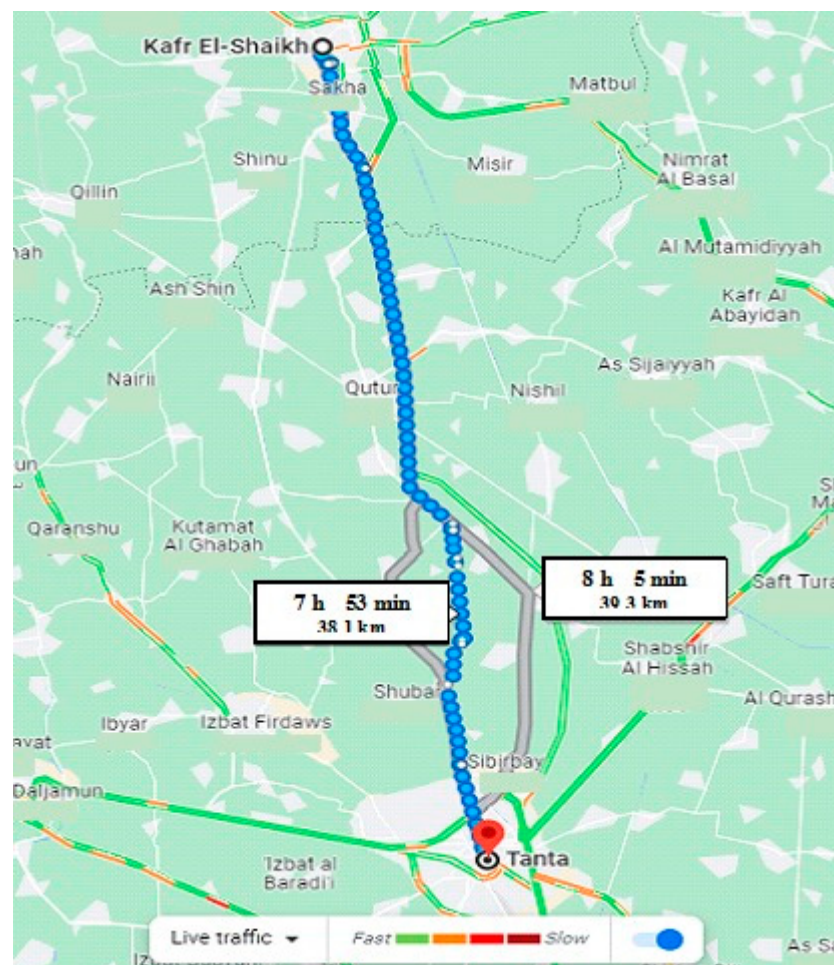
Figure 3. Investigated road (Kafr el sheikh–Tanta) in Egypt.

In May 2020, a field visit was arranged to inspect the road surface defects. The traditional visual inspection method for pavement evaluation was used. The road was divided into different segments (8 segments), and some tools were used, such as 30 m steel tape and paper sheet, to determine the density and severity of each distress. Then the data was recorded and analyzed. It was found that the road has several types of defects, such as alligator cracks, longitudinal cracks, roughness, patching, holes, and rutting, as illustrated in Figure 4. After five months (October 2020), a second visit was conducted, and it was found from visual inspection that the severity and density of defects had increased and became clearer. The dimensions of each defect are increased.

Figure 4. Surface distress of pavement based on visual inspection.

4. Results and Discussion

This section presents the findings and analysis of TLS data to define road condition assessment. The following results can be deduced based on TLS observations processing and analysis.

4.1. Flexible Pavement Defects

The area of defects in the flexible pavement (road) surface was discovered to be approximately eight positions of flexible pavements. According to the Egyptian code of practice for urban and rural roads [37], the defects were classified into four categories (cracking, surface deformation, roughness, and miscellaneous distresses). Table 2 presents in detail the faults in the positions.

The software used for TLS observations analysis is the MAGNET Collage program which allows data processing for a wide range of datasets, including laser scanning, mapping, and picture point retraction. To further simplify data collection, point coordinates should be applied to rapidly fit point clouds from terrestrial and sweep control. As il-

lustrated in Figure 5, it provides a good browsing experience with simple measurement and annotation tools such as split screen, filtered views, and linear spacing. It should be noted that the images in Figure 5were generated by MAGNET program based on TLS observations, and the images are 3D point cloud. The difference in colors in these images represents a change in the levels of these points, which facilitates the measurement process from each image.

Table 2. Types of distresses of the flexible pavement surface from laser scanner observations analysis.

| Distress Type	TLS Positions (Direction Kafr el Sheikh City to Tanta City)					TLS Positions (Direction Tanta to Kafr el Sheikh)			
	Pos 1	Pos 2 Left	Pos 3	Pos 4	Pos 5	Pos 2 Right	Pos 6	Pos 7	Pos 8
1. Cracking									
Alligator cracking				Yes	Yes	Yes			
Block cracking			Yes	Yes				Yes	
Edge cracking		Yes	Yes			Yes	Yes		
Longitudinal cracking	Yes	Yes	Yes	Yes	Yes	Yes			
Transverse cracking	Yes		Yes						
Slidage cracking		Yes				Yes			Yes
2. Surface deformation									
Rutting		Yes							
Depression									
Shoving		Yes		Yes		Yes	Yes		Yes
Corrugations									
Swelling									
Sags and bumps									Yes
Lane-to-shoulder dropoff		Yes				Yes			Yes
3. Roughness									
Bleeding	Yes			Yes	Yes				
Polished aggregate		Yes				Yes			
4. Miscellaneous distresses									
Raveling	Yes	Yes	Yes		Yes	Yes	Yes	Yes	Yes
Potholes	Yes	Yes	Yes		Yes	Yes			
Patching					Yes				
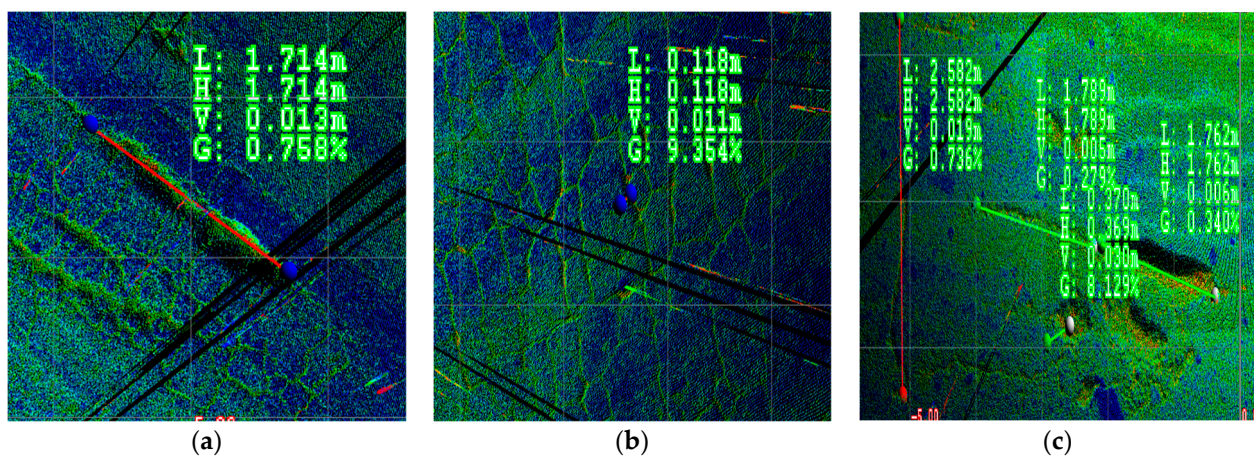
Figure 5. Samples for measured road surface distresses from laser scanner observations analysis Using MAGNET Collage program. Where: L: slope distance (m); H: horizontal distance (m); V: vertical distance (m); G: slope grade, (**a**) Longitudinal cracking in pos. 5, (**b**) Alligator cracking in pos. 6, (**c**) Longitudinal cracking and potholes in pos. 1.

Figure 6 demonstrates an example of measuring road surface defects based on visual inspection.
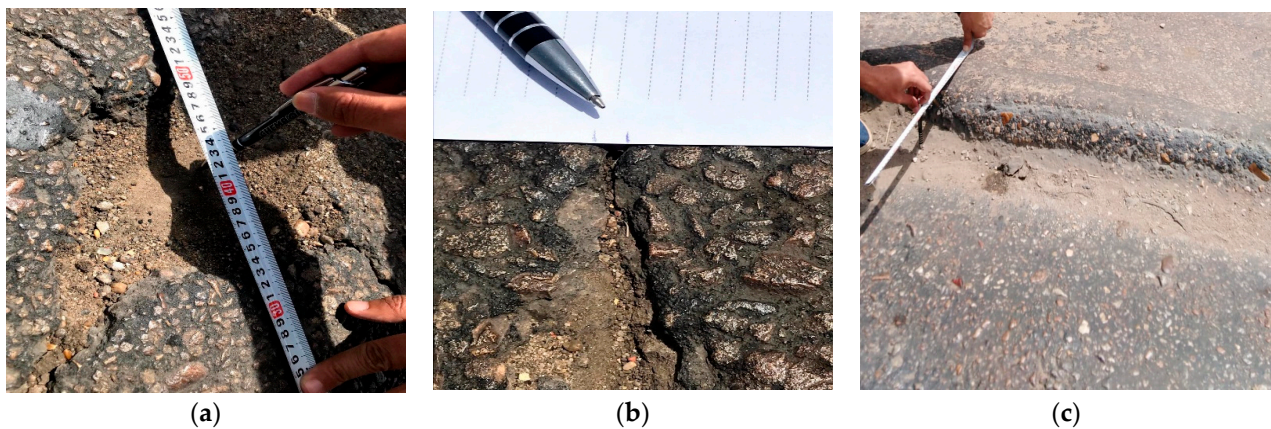

| (a) | (b) | (c) |

Figure 6. Measurement of road surface defects based on visual inspection. (**a**) Measuring Pothole's depth and width in pos.1, (**b**) Measuring block Cracking width in pos.3, (**c**) Measuring depth of lane to shoulder Dropoff in pos.2.

Table 3 compares the two measurement methods (MAGNET Collage program and visual inspection) of road surface defects. A visual inspection was conducted for each position, the inspector determined the type and severity of each distress, and the data was recorded in the inspection sheet. It can be noted that the results of the two methods are very close for the different road sections for most pavement distresses. It is also observed that the surface area of pothole distress was determined by the TLS method, which is considered more precise in evaluating the pavement conditions compared to counting the number of potholes conducted by the visual inspection method.

Table 3. Comparison of surface defect measurements by visual inspection and MAGNET Collage program from laser scanner observations.

| Position/Road Section No. | Type of Defect | Defect Value | | Error |
		Visual Inspection	TLS Observations	
Pos.1/Sec. 1	Longitudinal cracking	1.90 m	1.929 m	0.029 m
	Transverse cracking	2.25 m	2.287 m	0.037 m
	Bleeding	5.5 m^2	5.896 m^2	0.396 m^2
	Raveling	29.7 m^2	29.355 m^2	0.345 m^2
	Potholes	3 Potholes	(0.46, 0.31, 0.73) m^2	NA
Pos.2/Sec. 2	Edge Cracking	4 m	10.441 m	6.441 m
	Longitudinal cracking	(2 m × 1 cm)	14.199 m	NA
	Slidage cracking	16.85 m^2	16.962 m^2	0.112 m^2
	Shoving	4.20 m	4.226 m	0.026 m
	Lane-to-shoulder drop-off	10.2 m	10.990 m	0.79 m
	Polished aggregate	288 m^2	288.12 m^2	0.12 m^2
	Raveling	27.5 m^2	28.30 m^2	0.80 m^2
	Potholes	2 Potholes	(0.26, 0.45) m^2	NA
	Rutting	6 mm	6.226 mm	0.226 mm

Table 3. *Cont.*

Position/Road Section No.	Type of Defect	Defect Value		Error
		Visual Inspection	TLS Observations	
Pos.3/Sec. 3	Block cracking	2.73 m^2	2.735 m^2	0.005 m^2
	Longitudinal cracking	2.40 m	2.420 m	0.020 m
	Transverse cracking	2.50 m	2.532 m	0.032 m
	Raveling	12.97 m^2	12.835 m^2	0.135 m^2
	Potholes	3 Potholes	0.21, 0.37, 0.19 m^2	NA
	Edge cracking	12.60 m	12.615 m	0.015 m
Pos.4/Sec. 4	Alligator cracking	54 m^2	54.125 m^2	0.125 m^2
	Block cracking	1.15 m^2	1.150 m^2	0.0
	Bleeding	83.1 m^2	82.280 m^2	0.82 m^2
	Longitudinal cracking	15.40 m	15.477 m	0.077 m
	Shoving	7 mm	7.845 mm	0.845 mm
Pos.5/Sec. 5	Alligator cracking	6.40 m^2	6.436 m^2	0.036 m^2
	Longitudinal cracking	4.10 m	4.140 m	0.040 m
	Raveling	6.4 m^2	6.536 m^2	0.136 m^2
	Potholes	1 Pothole	0.36 m^2	NA
	Patching	1 Patching	28.738 m^2	NA
Pos.6/Sec. 6	Alligator cracking	60.70 m^2	60.737 m^2	0.037 m^2
	Edge cracking	7.20 m	7.251 m	0.051 m
	Raveling	65.70 m^2	65.745 m^2	0.045 m^2
	Shoving	10 mm	10.036 mm	0.036 mm
Pos.7/Sec. 7	Block cracking	250 m^2	256.52 m^2	1.52 m^2
	Raveling	230 m^2	235.68 m^2	5.68 m^2
Pos.8/Sec. 8	Slidage cracking	80.6 m^2	79.277 m^2	1.323 m^2
	Shoving	5 mm	5.994 mm	0.994 mm
	Sags and pumps	14 m^2	14.968 m^2	0.968 m^2
	Lane-to-shoulder drop-off	3.5 m	3.564 m	0.064 m
	Raveling	15 m^2	15.964 m^2	0.964 m^2

NA = Not applicable.

4.2. Geometric Properties of Road Cross Section

The geometric dimensions of the investigated roads for each position were determined based on the TLS measurements, as presented in Table 4. The accuracy of road and shoulder width measurements obtained from TLS observations processing ranged from 2 mm to 11 mm compared with the actual road dimensions. It can be observed that the average width of carriage lanes is 7.5 m and 1.60 m for the shoulder.

The longitudinal and cross-section slope angles were calculated for all TLS positions based on the laser scanner observations (cloud of points coordinates). The values are displayed in Table 5, and it can be seen that the longitudinal slope angles vary from $0°18'7.2''$ at Position 4 to $1°17'13.20''$ at Position 2; however, the values of cross-section slope angles are greater than the longitudinal slope where it varies from $0°51'21.60''$ at position 2 to $7°5'56.4''$ at position 1.

Table 4. Dimensions of road and shoulder width at each section.

Positions (Sections) of TLS	Average of Road Width, (m)	Average Shoulder Width, (m)
Pos.1	7.213	1.711
Pos.2	7.501	1.470
Pos.3	7.402	1.453
Pos.4	7.412	1.513
Pos.5	7.532	1.632
Pos.6	7.497	1.515
Pos.7	7.499	1.598
Pos.8	7.513	1.498

Table 5. Values of longitudinal and cross-section slope angles for all TLS positions.

Distance	Direction (From–to)	Longitudinal Slope Angle	Cross Section Slope Angle
Pos. 1 (0.00) km	Kafr el sheikh–Tanta	0°57'7.20''	7°5'56.4''
Pos. 2 (5.89) km	Intersection	1°17'13.20''	0°51'21.60''
Pos. 3 (6.574) km	Kafr el sheikh–Tanta	0°9'46.8''	5°15'8''
Pos. 4 (7.117) km	Tanta–Kafr el sheikh	0°18'7.2''	3°11'37.2''
Pos. 5 (10.277) km	Kafr el sheikh–Tanta	0°12'28.80''	4°7'33.6''
Pos. 6 (15.467) km	Tanta–Kafr el sheikh	0°39'25.2''	1°45'2''
Pos. 7 (15.888) km	Kafr el sheikh–Tanta	0°22'51.6''	3°0'14.6''
Pos. 8 (25.177) km	Tanta–Kafr el sheikh	0°5'46.2''	2°46'41.2''

4.3. Pavement Conditions Index

The pavement conditions are determined by the PCI method, which is indicated by a number ranging between 0 and 100, where 0 means the worst pavement condition and 100 indicates the best condition. The PCI depends on the distresses identified during inspections and indicates the surface condition [38,39].

In addition to PCI, values can be used to prepare the priorities and the required budget for performing pavement maintenance and rehabilitation (M&R) programs. The PCI can be conducted by the traditional process, which is the visual inspection. In this case, there is a concern related to road safety and human errors, affecting the calculations' accuracy [39,40]. PAVER software was used to determine the PCI values for each section depending on the results of TLS observations for road defects. The distance between each TLS position and the other position was divided into a longitudinal section of the road, and the average value of PCI was calculated for each section.

Table 6 displays the average estimated values of PCI for the different sections based on the TLS observations and the traditional visual inspection method. It can be noted from Table 6 that the maximum value of PCI is equal to 70 and more for all positions except positions (two and five) for the two methods of measurement, which indicates a very good index of the pavement surface. However, the pavement condition index for positions two and five is very poor, as the estimated value for PCI is less than 25. It can also be observed from the table the value of PCI based on TLS data is almost the same as the visual inspection method, which confirms the accuracy of TLS observation in determining the pavement defects. A maintenance program should be proposed based on the pavement conditions index, especially Sections 2 and 5.

Table 6. Average values of PCI from TLS observation and visual inspection method.

Section (Position) No.	Average PCI Value		Pavement Condition
	TLS Observations	**Visual Inspection**	
1	Very good	71	73
2	Very poor	10	11
3	Very good	71	70
4	Very good	70	70
5	Very poor	21	23
6	Very good	70	73
7	Very good	71	70
8	Very good	72	70

4.4. Surface Deformation of Pavement

The investigated road positions are assumed to be flat (plane). The plane equation was computed by applying the least squares method to determine the surface deformation of each position concerning the result in the fitted plane for each instrument position. Table 7 provides the maximum and minimum surface deformations values for each TLS position to the resulting plane fitting. It was found that the maximum and minimum values for the surface were 50.74 mm and 2.05 mm, respectively.

Table 7. Statistical values of surface deformation for each section (position) of TLS.

TLS Section (Position) No.	Maximum Deformation, (mm)	Minimum Deformation, (mm)	Average Deformation, (mm)
Pos.1	11.23	2.25	7.293
Pos.2	50.74	3.35	28.07
Pos.3	24.77	3.69	13.67
Pos.4	31.16	3.85	18.59
Pos.5	35.24	2.26	18.37
Pos.6	38.80	3.31	21.02
Pos.7	42.12	2.91	22.96
Pos.8	44.13	2.05	24.69

5. Conclusions

This paper explored the use of TLS observations for determining pavement distresses and assessing the quality of pavement surface for a major road (Kafr EL-Sheikh–Tanta road, Egypt) having a length of 20 km. It illustrates one of the main concepts for the pavement management system (PMS), which is carefully employed in the investigated road. In this research, the data was analyzed by dividing the TLS resulting in the point cloud into eight sub-clouds (one for each instrument position) and determining the equation of planes for the different positions and the general plane. Based on the provided experimental, site work, and analysis, the following conclusions can be drawn:

1. The proposed applied technique of employing TLS for observing and monitoring the pavement surface conditions and determining the surface distresses has proven effective, significant, and accurate compared to the traditional evaluation methods. It represents an effective method for data collection to detect pavement distress As a result, TLS can be a good alternative to traditional techniques and visual inspection for detecting flexible pavement defects, as it saves effort and money and does not cause any traffic disruption. For visual inspection, the work can take a long time, approaching several days, in addition to the involvement of several technicians to complete the visual examination and measure the defects manually. However, the use of the laser scanner took place in a few hours and provided an acceptable accuracy of

determining the defects and their dimensions compared to the traditional methods. Consequently, the reliability of the work is improved and helpful in determining the optimal methods for maintaining these defects.

2. The monitored road (a case study for flexible pavement) has several apparent defects in the upper surface. Therefore, these defects must be repaired using an engineering and technical technique following international specifications. The maximum deformation value in the investigated road reaches 50.74 mm, and the minimum value is 2.05 mm, with an average value of 19.4 mm along the longitudinal section of the road (through 20 km long).Using the plane equation method and finding the distortion of each point represents an effective technique for calculating the deformation of any vertical or horizontal surface, particularly from TLS observations, as long as the observations are treated by applying the least square estimation technique, as described in this research.

3. The findings of this study will be helpful for decision-makers, especially in the case of conducting pavement maintenance on the investigated road. In addition, using this device (laser scanner) saves time and effort with acceptable accuracy in identifying pavement defects.

Author Contributions: Conceptualization, A.A. and A.A.A.B.; methodology, A.A., M.A. and M.M.E.-B.; software, M.M.E.-B., A.A.A.B and A.A.; validation, A.M.Y., M.M.E.-B. and M.A.; formal analysis, A.A., A.H.A. and A.A.A.B.; investigation, A.A.; resources, M.A. and M.M.E.-B.; data curation, A.A.A.B.; writing—original draft, A.A., M.A., A.H.A. and A.A.A.B and M.M.E.-B.; writing—review and editing, A.A. and M.M.E.-B.; visualization, M.A., A.H.A. and M.M.E.-B. All authors have read and agreed to the published version of the manuscript.

Data Availability Statement: Data are included within the article.

Conflicts of Interest: The authors declare that they have no known competing financial interests or personal relationships that could have appeared to influence the work reported in this paper.

References

1. Arab, M.G.; Alzara, M.; Zeiada, W.; Omar, M.; Azam, A. Combined effect of compaction level and matric suction conditions on flexible pavement performance using construction and demolition waste. *Constr. Build. Mater.* **2020**, *261*, 119792. [CrossRef]
2. Mousa, E.; El-Badawy, S.; Azam, A. Effect of reclaimed asphalt pavement in granular base layers on predicted pavement performance in Egypt. *Innov. Infrastruct. Solut.* **2020**, *5*, 57. [CrossRef]
3. Baldo, N.; Miani, M.; Rondinella, F.; Manthos, E.; Valentin, J. Road Pavement Asphalt Concretes for Thin Wearing Layers: A Machine Learning Approach towards Stiffness Modulus and Volumetric Properties Prediction. *Period. Polytechnica. Civ. Eng.* **2022**, *66*, 1087–1097. [CrossRef]
4. Ragnoli, A.; De Blasiis, M.R.; Di Benedetto, A. Pavement Distress Detection Methods: A Review. *Infrastructures* **2018**, *3*, 58. [CrossRef]
5. Bella, F.; Calvi, A.; D'amico, F. Impact of Pavement Defects on Motorcycles' Road Safety. *Procedia Soc. Behav. Sci.* **2012**, *53*, 942–951. [CrossRef]
6. Simões, D.; Almeida-Costa, A.; Benta, A. Preventive maintenance of road pavement with microsurfacing—An economic and sustainable strategy. *Int. J. Sustain. Transp.* **2017**, *11*, 670–680. [CrossRef]
7. Issa, A.; Samaneh, H.; Ghanim, M. Predicting pavement condition index using artificial neural networks approach. *Ain Shams Eng. J.* **2021**, *13*, 101490. [CrossRef]
8. Schwartz, C.W.; Li, R.; Ceylan, H.; Kim, S.; Gopalakrishnan, K. Global Sensitivity Analysis of Mechanistic–Empirical Performance Predictions for Flexible Pavements. *Transp. Res. Rec.* **2013**, *2368*, 12–23. [CrossRef]
9. Kim, M.-K.; Sohn, H.; Chang, C.-C. Localization and Quantification of Concrete Spalling Defects Using Terrestrial Laser Scanning. *J. Comput. Civ. Eng.* **2015**, *29*, 04014086. [CrossRef]
10. Azam, A.M.; El-Badawy, S.M.; Alabasse, R.M. Evaluation of asphalt mixtures modified with polymer and wax. *Innov. Infrastruct. Solut.* **2019**, *4*, 43. [CrossRef]

11. Tarbay, E.W.; Azam, A.M.; El-Badawy, S.M. Waste materials and by-products as mineral fillers in asphalt mixtures. *Innov. Infrastruct. Solut.* **2019**, *4*, 5. [CrossRef]

12. Yang, X.; You, Z.; Hiller, J.; Watkins, D. Sensitivity of flexible pavement design to Michigan's climatic inputs using pavement ME design. *Int. J. Pavement Eng.* **2015**, *18*, 622–632. [CrossRef]

13. Zapata, C.E.; Salim, R.A. Impact of Environmental Site Location and Groundwater Table Depth on Thickness of Flexible Airfield Pavements. *Transp. Res. Rec.* **2012**, *2282*, 22–33. [CrossRef]

14. Zapata, C.; Andrei, D.; Witczak, M.; Houston, W. Incorporation of Environmental Effects in Pavement Design. *Road Mater. Pavement Des.* **2007**, *8*, 667–693. [CrossRef]

15. Beshr, A.A.A.; Heneash, O.G.; Fawzy, H.E.-D.; El-Banna, M.M. Condition assessment of rigid pavement using terrestrial laser scanner observations. *Int. J. Pavement Eng.* **2021**, *23*, 4248–4259. [CrossRef]

16. Beshr, A. *Monitoring the Structural Deformation of Tanks*; LAP LAMBERT Academic Publishing: Saarbrücken, Germany, 2012; ISBN 978-3-659-29943-8.

17. Barbieri, G.; da Silva, F.P. Acquisition of 3D models with submillimeter-sized features from SEM images by use of photogrammetry: A dimensional comparison to microtomography. *Micron* **2019**, *121*, 26–32. [CrossRef] [PubMed]

18. Barbarella, M.; D'amico, F.; De Blasiis, M.R.; Di Benedetto, A.; Fiani, M. Use of Terrestrial Laser Scanner for Rigid Airport Pavement Management. *Sensors* **2017**, *18*, 44. [CrossRef]

19. Feng, Z.; El Issaoui, A.; Lehtomäki, M.; Ingman, M.; Kaartinen, H.; Kukko, A.; Savela, J.; Hyyppä, H.; Hyyppä, J. Pavement Distress Detection Using Terrestrial Laser Scanning Point Clouds—Accuracy Evaluation and Algorithm Comparison. *ISPRS Open. J. Photogramm. Remote. Sens.* **2022**, *3*, 100010. [CrossRef]

20. El Issaoui, A.; Feng, Z.; Lehtomäki, M.; Hyyppä, E.; Hyyppä, H.; Kaartinen, H.; Kukko, A.; Hyyppä, J. Feasibility of Mobile Laser Scanning towards Operational Accurate Road Rut Depth Measurements. *Sensors* **2021**, *21*, 1180. [CrossRef]

21. Bitelli, G.; Simone, A.; Girardi, F.; Lantieri, C. Laser Scanning on Road Pavements: A New Approach for Characterizing Surface Texture. *Sensors* **2012**, *12*, 9110–9128. [CrossRef] [PubMed]

22. Mitchell; Chang, J.-R.; Chang, K.-T.; Chen, D.-H. Application of 3D Laser Scanning on Measuring Pavement Roughness. *J. Test. Eval.* **2006**, *34*, 83–91. [CrossRef]

23. Chang, K.T.; Chang, J.R.; Liu, J.K. Detection of Pavement Distresses Using 3D Laser Scanning Technology. In Proceedings of the International Conference on Computing in Civil Engineering 2005, Cancun, Mexico, 12–15 July 2005. [CrossRef]

24. De Blasiis, M.R.; Di Benedetto, A.; Fiani, M. Mobile Laser Scanning Data for the Evaluation of Pavement Surface Distress. *Remote Sens.* **2020**, *12*, 942. [CrossRef]

25. Lueangvilai, E. Development of Structure and Pavement Inspection Using Mobile Laser Scanning Point Clouds: A Case Study of Thailand Expressway. Ph.D. Thesis, Thammasat University, Bangkok, Thailand, 2022.

26. Yi, T.J.; Ahmad, A.B. Quality Assessments of Unmanned Aerial Vehicle (UAV) and Terrestrial Laser Scanning (TLS) Methods in Road Cracks Mapping. *Int. Arch. Photogramm. Remote Sens. Spat. Inf. Sci.* **2023**, *48*, 183–193. [CrossRef]

27. Llopis-Castelló, D.; García-Segura, T.; Montalbán-Domingo, L.; Sanz-Benlloch, A.; Pellicer, E. Influence of Pavement Structure, Traffic, and Weather on Urban Flexible Pavement Deterioration. *Sustainability* **2020**, *12*, 9717. [CrossRef]

28. Tarawneh, S.; Sarireh, M. Causes of Cracks and Deterioration of Pavement on Highways in Jordan from Contractors' Perspective. *Civ. Environ. Res.* **2013**, *3*, 16–27.

29. Tsai, Y.; Wu, Y.; Doan, J. A critical assessment of jointed plain concrete pavement (JPCP) using sensing technology—A case study on I-285. In Proceedings of the 9th International Conference on Managing Pavement Assets, Alexandria, VA, USA, 18–22 May 2015.

30. Darter, M.; Khazanovich, L.; Yu, T.; Mallela, J. Reliability Analysis of Cracking and Faulting Prediction in the New Mechanistic–Empirical Pavement Design Procedure. *Transp. Res. Rec.* **2005**, *1936*, 150–160. [CrossRef]

31. Tsai, Y.J.; Wu, Y.; Ai, C. Feasibility study of measuring concrete joint faulting using 3d continuous pavement profile data 2. In Proceedings of the Transportation Research Board 90th Annual Meeting, Washington, DC, USA, 23–27 January2011.

32. McGhee, K.H. *Automated Pavement Distress Collection Techniques*; Transportation Research Board: Washington, DC, USA, 2004.

33. Jung, Y.S.; Zollinger, D.G. New Laboratory-Based Mechanistic–Empirical Model for Faulting in Jointed Concrete Pavement. *Transp. Res. Rec.* **2011**, *2226*, 60–70. [CrossRef]

34. Mraz, A.; Nazef, A.; Lee, H.; Holzschuher, C.; Choubane, B. Precision of Florida Methods for Automated and Manual Faulting Measurements. *Transp. Res. Rec.* **2012**, *2306*, 131–137. [CrossRef]

35. Available online: https://topconsokkia.ind.in/topcon-brand/laser-scanner/software/magnet-collage (accessed on 11 April 2023).

36. Khullar, R.; Mishra, G.; Sharma, G.; Prakash, B.; Gehlot, M.; Huse, V.; Mishra, S. A polygon laser scanning micrometer for magnet size measurement studies. *J. Instrum.* **2014**, *9*, T05003. [CrossRef]

37. *ECP Egyptian Code of Practice for Urban and Rural Roadspart 10: Road Maintenance*; Housing and Building National Research Center: Dokki, Egypt, 2018.

38. Loprencipe, G.; Pantuso, A.; Di Mascio, P. Sustainable Pavement Management System in Urban Areas Considering the Vehicle Operating Costs. *Sustainability* **2017**, *9*, 453. [CrossRef]

39. Karballaeezadeh, N.; Zaremotekhases, F.; Shamshirband, S.; Mosavi, A.; Nabipour, N.; Csiba, P.; Várkonyi-Kóczy, A.R. Intelligent Road Inspection with Advanced Machine Learning; Hybrid Prediction Models for Smart Mobility and Transportation Maintenance Systems. *Energies* **2020**, *13*, 1718. [CrossRef]
40. Karballaeezadeh, N.; Mohammadzadeh, S.D.; Moazemi, D.; Band, S.S.; Mosavi, A.; Reuter, U. Smart Structural Health Monitoring of Flexible Pavements Using Machine Learning Methods. *Coatings* **2020**, *10*, 1100. [CrossRef]